

## Mg Segregation at Al/Al<sub>3</sub>Sc Heterophase Interfaces on an Atomic Scale: Experiments and Computations

E. A. Marquis,<sup>1,\*</sup> D. N. Seidman,<sup>1</sup> M. Asta,<sup>1</sup> C. Woodward,<sup>1,†</sup> and V. Ozoliņš<sup>2</sup>

<sup>1</sup>*Department of Materials Science and Engineering, Northwestern University, Evanston, Illinois 60208, USA*

<sup>2</sup>*Department of Materials Science and Engineering, University of California, Los Angeles, California 90095, USA*

(Received 8 March 2003; published 18 July 2003)

Microscopic factors governing solute partitioning in ternary two-phase Al-Sc-Mg alloys are investigated combining three-dimensional-atom-probe (3DAP) microscopy measurements with first-principles computations. 3DAP is employed to measure composition profiles with subnanometer-scale resolution, leading to the identification of a large enhancement of Mg solute at the coherent  $\alpha$ -Al/Al<sub>3</sub>Sc (fcc/L1<sub>2</sub>) heterophase interface. First-principles calculations establish an equilibrium driving force for this interfacial segregation reflecting the nature of the interatomic interactions.

DOI: 10.1103/PhysRevLett.91.036101

PACS numbers: 68.35.Dv, 68.35.Md

Structural alloys typically contain multiple alloying elements whose interactions govern the formation of strengthening phases, partitioning behavior, and segregation at internal interfaces. Through the combination of high resolution electron microscopy (HREM) and three-dimensional atom-probe (3DAP) microscopy, it has become possible recently to measure compositional variations with near-atomic-scale resolution. The combined application of such characterization techniques with first-principles computational methods provides the basis for greatly expanded insight into the microscopic factors governing compositional distributions in multi-component alloys. The present work employs such a combined approach in a study of Mg in two-phase Al-Sc-Mg alloys. We present measurements of Mg composition profiles at the subnanoscale level, which are compared to the predictions of first-principles calculations. These calculations establish a pronounced electronic driving force for the segregation of Mg to coherent Al/Al<sub>3</sub>Sc interfaces in this model two-phase ternary alloy system.

We focus on an Al-2.2 at. % Mg-0.12 at. % Sc alloy, interesting both for aerospace applications [1] and as a model system for its microstructural properties. The alloy was prepared employing solidification and homogenization procedures outlined previously [2,3]. During aging at 300 °C, the supersaturated solid solution decomposes into an  $\alpha$ -Al matrix and a high number density ( $4 \pm 2 \times 10^{22}$  precipitate m<sup>-3</sup>) of nanoscale Al<sub>3</sub>Sc precipitates with radii less than 4.5 nm. HREM observations demonstrate that the  $\alpha$ -Al/Al<sub>3</sub>Sc interface remains coherent in both the binary Al-0.18 at. % Sc and ternary Al-Mg-Sc alloys even for the largest precipitates with radii of 4.5 nm. Without Mg, the precipitate shows pronounced facets on the {100}, {110}, and {111} planes [2] [Fig. 1(A)], which tend to shrink [Fig. 1(B)] with addition of Mg. The reduction of {100} facet lengths with the addition of Mg suggests a decrease in the crystallographic anisotropy of the interfacial free energy and the possibility of appreciable interfacial segregation. To investigate the behavior

of Mg further, we have undertaken detailed 3DAP measurements of solute composition profiles.

The spatial resolution of the 3DAP is illustrated in Fig. 2(A), where an analysis performed near the 110 crystallographic pole reveals the {220} atomic planes perpendicular to the analysis direction. The curvature of the reconstructed planes comes from the projection of the hemispherical tip onto a planar detector. In the Al<sub>3</sub>Sc precipitate, alternating planes containing 100% Al and 50% Al are visible, consistent with the L1<sub>2</sub> structure of the Al<sub>3</sub>Sc phase. A proximity histogram calculates average composition in shells of 0.4 nm thickness at different distances from the  $\alpha$ -Al/Al<sub>3</sub>Sc interface; the

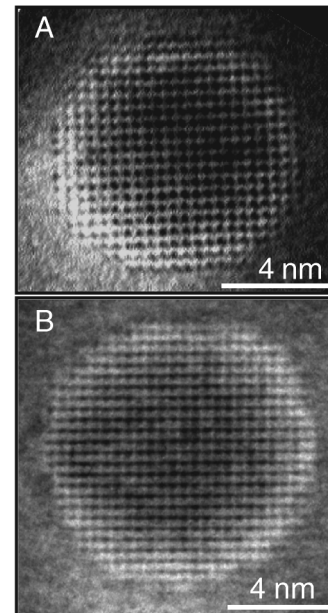


FIG. 1. HREM images ([100] zone axis) of Al<sub>3</sub>Sc precipitates in (A) Al-0.18 at. % Sc alloy after aging at 300 °C for 350 h; and (B) Al-2.2 at. % Mg-0.12 at. % Sc after aging at 300 °C for 1040 h.

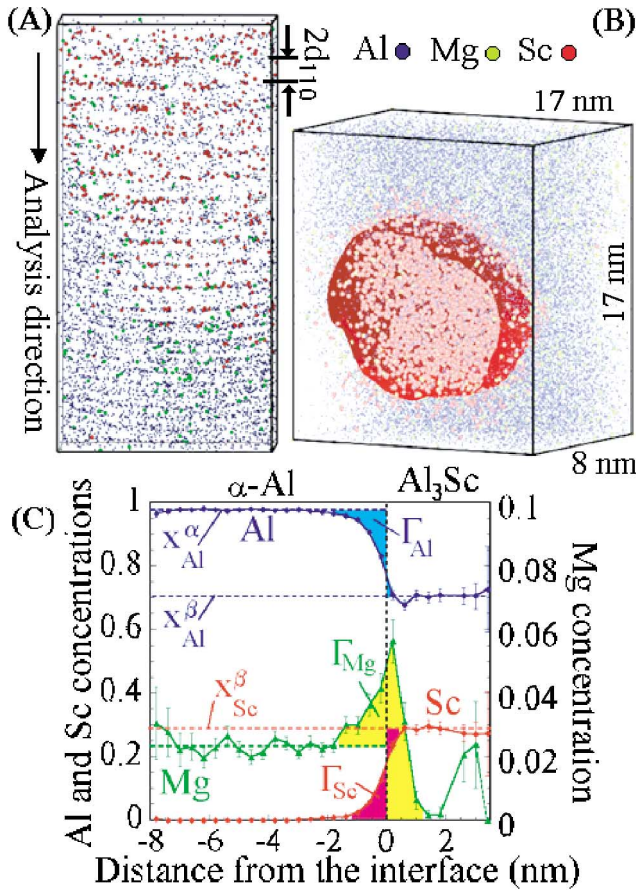


FIG. 2 (color). (A) 3D reconstruction of an Al<sub>3</sub>Sc precipitate with a slice taken through the precipitate showing the {110} planes. (B) 3D reconstruction of an analyzed volume from a tip aged at 300 °C for 1040 h showing the isoconcentration surface used to define the  $\alpha$ -Al/Al<sub>3</sub>Sc heterophase interface. Sc (Mg) atoms are in pink-red (light green), and Al in blue. (C) Proximity histogram showing Al, Mg, and Sc concentrations with respect to distance from the  $\alpha$ -Al/Al<sub>3</sub>Sc interface. Data visualization performed using the ADAM 1.5 software [4].

interface is defined by an isoconcentration surface corresponding to 18 at. % Sc [Fig. 2(B)] [4]. Interfacial Mg segregation was observed for all analyzed aging times, and the particular example of Fig. 2(C) exhibits a Mg concentration enhancement at the interface of 180%. The maximum interface Mg concentration slightly decreases during the early aging times, then remains constant within experimental error.

To investigate the microscopic factors governing the pronounced measured interfacial enhancement of Mg, we first employ the theoretical framework provided by a model of diffusion-limited precipitate growth kinetics. The validity of such a model is supported by studies of coarsening kinetics in both binary Al-Sc [2,5,6] and ternary Al-Sc-Mg [3] alloys. We thus interpret the composition profiles measured by 3DAP as representing steady-state solutions to the diffusion equation, subject

to the boundary conditions imposed by local thermodynamic equilibrium and flux balance at the growing interface (e.g., [7]). For spherical precipitate geometries, employing a mean-field, steady-state solution to the diffusion equation (neglecting off-diagonal terms in the diffusion matrix), interface compositions can be derived from the following equations [7] ( $i = \text{Al, Sc, Mg}$ ):

$$\mu_i^\alpha(\hat{x}_{\text{Mg}}^\alpha, \hat{x}_{\text{Sc}}^\alpha) - \mu_i^{\alpha'}(\hat{x}_{\text{Mg}}^{\alpha'}, \hat{x}_{\text{Sc}}^{\alpha'}) = \frac{2\sigma}{R} \bar{V}_i, \quad (1)$$

$$\frac{\hat{x}_{\text{Sc}}^{\alpha'} - \hat{x}_{\text{Sc}}^\alpha}{\hat{x}_{\text{Mg}}^{\alpha'} - \hat{x}_{\text{Mg}}^\alpha} = \frac{D_{\text{Sc}}}{D_{\text{Mg}}} \frac{\hat{x}_{\text{Sc}}^\alpha - \hat{x}_{\text{Sc}}^\infty}{\hat{x}_{\text{Mg}}^\alpha - \hat{x}_{\text{Mg}}^\infty}, \quad (2)$$

where  $\hat{x}_{\text{Sc}}^\alpha$ ,  $\hat{x}_{\text{Mg}}^\alpha$ ,  $\hat{x}_{\text{Sc}}^{\alpha'}$ , and  $\hat{x}_{\text{Mg}}^{\alpha'}$  denote mole fractions of Sc and Mg on the Al ( $\alpha$ ) and Al<sub>3</sub>Sc ( $\alpha'$ ) sides of the interface for a precipitate of radius  $R$ .  $\sigma$  is the interfacial free energy, the variables  $\mu_i^\alpha$  and  $\mu_i^{\alpha'}$  represent bulk chemical potentials, and  $\bar{V}_i$  is the partial molar volume for species  $i$  in the precipitate phase. The variables  $x_{\text{Sc}}^\infty$  and  $x_{\text{Mg}}^\infty$  denote far-field matrix solute concentrations. The first three equations [Eq. (1)] correspond to the Gibbs-Thomson conditions incorporating the effect of capillarity in the formulation of the conditions for local thermodynamic equilibrium, while Eq. (2) reflects the constraint imposed by solute flux balance at the precipitate/matrix interface.

Table I lists values of the interface concentrations calculated from Eqs. (1) and (2) for precipitates of radii 2 and 4 nm at an aging temperature of 300 °C. For comparison, we also list compositions corresponding to two-phase equilibrium between bulk ( $R \rightarrow \infty$ )  $\alpha$  and  $\alpha'$  phases in the ternary alloy Al-2.2 at. % Mg-0.12 at. % Sc considered experimentally. Since experimental values for the chemical potentials in the ternary Al<sub>3</sub>Sc intermetallic phase are unavailable, we have employed first-principles bulk free-energy models in the calculations of equilibrium phase compositions. The bulk free energies were derived within a model of noninteracting substitutional defects following the approach outlined in Refs. [8–10]. In the evaluation of Eq. (2), we employ 3DAP-measured values  $\hat{x}_{\text{Sc}}^\infty = 0.025 \pm 0.007$  at. % and  $\hat{x}_{\text{Mg}}^\infty = 2.3 \pm 0.007$  at. % [3]. The solute diffusivities in Al are  $D_{\text{Sc}} = 8.84 \times 10^{-20}$  m<sup>2</sup>/s [11] and  $D_{\text{Mg}} = 1.62 \times 10^{-16}$  m<sup>2</sup>/s [12]. Additionally, we employ the value  $\sigma = 0.175$  J/m<sup>2</sup> derived from first-principles calculations [13]. Values

TABLE I. Interface solute concentrations (at. %) calculated from Eqs. (1) and (2) for spherical ( $\alpha'$ ) Al<sub>3</sub>Sc precipitates of radius  $R$  growing in a supersaturated ( $\alpha$ ) Al matrix in Al-Sc-Mg.

$R$ (nm)	$\hat{x}_{\text{Sc}}^\alpha$	$\hat{x}_{\text{Mg}}^\alpha$	$\hat{x}_{\text{Sc}}^{\alpha'}$	$\hat{x}_{\text{Mg}}^{\alpha'}$
2	$2.5 \times 10^{-4}$	2.2	25	$3.4 \times 10^{-7}$
4	$1.8 \times 10^{-4}$	2.2	25	$4.0 \times 10^{-7}$
$\infty$	$9.0 \times 10^{-5}$	2.4	25	$4.8 \times 10^{-7}$

of the interface compositions for precipitates with finite radii were derived by linearizing the concentration dependencies of Eqs. (1) and (2) about the bulk compositions. By comparing the results in the first two rows of Table I with those corresponding to bulk phases (final row), we see that the effects of capillarity and solute flux balance are estimated to give rise to relatively small ( $\approx 10\%$ ) changes in the matrix Mg concentration at the growing precipitate/matrix interface. Thus, *the pronounced interfacial enhancement of Mg measured by 3DAP microscopy cannot be interpreted simply as reflecting the effects of capillarity and solute flux balance in a model of diffusion-limited precipitate growth.* Additional first-principles calculations suggest instead that the segregation of Mg observed by 3DAP microscopy reflects equilibrium interfacial adsorption.

First-principles calculations were conducted to investigate the energetics of Mg solute atoms in the vicinity of planar coherent  $\alpha$ -Al/Al<sub>3</sub>Sc interfaces aligned parallel to {200} crystallographic planes [14]. Figure 3(a) plots calculated formation energies ( $\Delta E$ ) for substituting Mg for Al as a function of distance from the coherent {200} Al/Al<sub>3</sub>Sc planar interface. The values of  $\Delta E$  calculated on the Al<sub>3</sub>Sc side of the interface are roughly 0.6 eV larger than in pure Al, indicative of the strong energetic preference for the partitioning of Mg to the matrix phase. In terms of the 3DAP measurements, the most important feature of the results shown in Fig. 3(a) is the negative value of  $\Delta E$  calculated on the Al side of the interface at the second-neighbor sites of the interface Sc atoms. The formation energy at these sites is computed to be 0.1 eV lower than the heat of solution for Mg atoms in bulk Al. This segregation energy provides a significant driving force for equilibrium Mg segregation at the coherent {200} Al/Al<sub>3</sub>Sc interface.

To make explicit contact with the 3DAP experimental results, the energies derived from the first-principles calculations have been used within a mean-field model for the configurational free energy to compute the equilibrium solute composition profiles across a planar  $\alpha$ -Al/Al<sub>3</sub>Sc {200} interface at 300 °C. From this analysis, we find negligible Mg solubility in the Al<sub>3</sub>Sc phase, and variations in the concentration on the Al side governed by the equation  $x_{\text{Mg}}/x_{\text{Mg}}^0 = \exp\{-[\Delta E - \Delta E(\infty)]/k_B T\}$  (neglecting vibrational contributions to the entropy). The planar-averaged Mg concentration profile is shown in Fig. 3(b), and features a five- to sixfold enhancement of  $x_{\text{Mg}}$  in the plane positioned one lattice constant from the interface Sc atoms. In comparison to the 3DAP microscopy results for Mg plotted in Fig. 2(C), the calculated concentration profile is narrower with a larger value for Mg enhancement. The measured concentration profile at the  $\alpha$ -Al/Al<sub>3</sub>Sc interface is probably wider than the real one due to trajectory effects associated with the field-evaporated ions [17], which act to broaden sharp composition peaks.

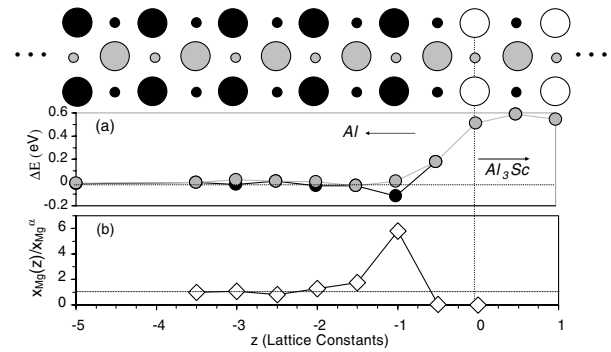


FIG. 3. The upper panel shows a projection of the interface atomic structure with black and gray circles denoting Al positions, and white circles corresponding to Sc sites. (a) Calculated formation energies ( $\Delta E$ ) for substitution of Mg for Al as a function of distance ( $z$ ) from an  $\alpha$ -Al/Al<sub>3</sub>Sc interface. (b) Calculated Mg concentration profile. Compositions have been normalized by the far-field matrix composition.

A more reliable comparison between experiment and theory can be made in terms of the integrated area under the Mg concentration profiles. Specifically, the relative segregation coefficient ( $\Gamma_{\text{Mg}}^{\text{rel}}$ ) of Mg can be employed to derive a quantitative measure of the degree of equilibrium Mg segregation in this ternary alloy. This coefficient can be calculated from  $\Gamma_{\text{Mg}}$ ,  $\Gamma_{\text{Sc}}$ , and  $\Gamma_{\text{Al}}$ , the interfacial excesses of Mg, Sc, and Al, as described in [18]. We estimate these excess values for Al (negative value), Mg, and Sc (positive values) as the areas under the concentration curves in the proximity histogram, as displayed in Fig. 2(C) [19]. This analysis of the experimental data yields  $\Gamma_{\text{Mg}}^{\text{rel}} = 1.9 \pm 0.5 \text{ atom nm}^{-2}$ . By comparison,  $\Gamma_{\text{Mg}}^{\text{rel}}$  derived from the calculated composition profiles is  $1.2 \text{ atom nm}^{-2}$ . The close agreement between experiment and theory strongly supports the conclusion that *the measured interfacial enhancement of Mg reflects pronounced equilibrium segregation of this species to coherent  $\alpha$ -Al/Al<sub>3</sub>Sc Sc heterophase interfaces.* From the Gibbs adsorption theorem, we estimate that Mg segregation leads to  $0.01 \text{ J/m}^2$  reduction in  $\sigma$ . Equilibrium interfacial segregation of Mg should thus reduce slightly (by approximately 5%) the rates of precipitate coarsening in Al-Sc-Mg relative to binary Al-Sc.

Insight into the microscopic origin of Mg interfacial segregation can be obtained by considering the calculated solute-solute interactions in Al plotted in Fig. 4. The large magnitude and oscillating nature of the Sc-Sc results are consistent with theoretical models for transition-metal electronic interactions in Al [20,21]. Both Sc-Sc and Mg-Sc interactions are repulsive at first and third neighbors, and attractive at second and fourth. The overall magnitude of the calculated segregation energy, as well as the preferred binding site for Mg at the  $\alpha$ -Al/Al<sub>3</sub>Sc {200} interface, can thus be rationalized as follows.

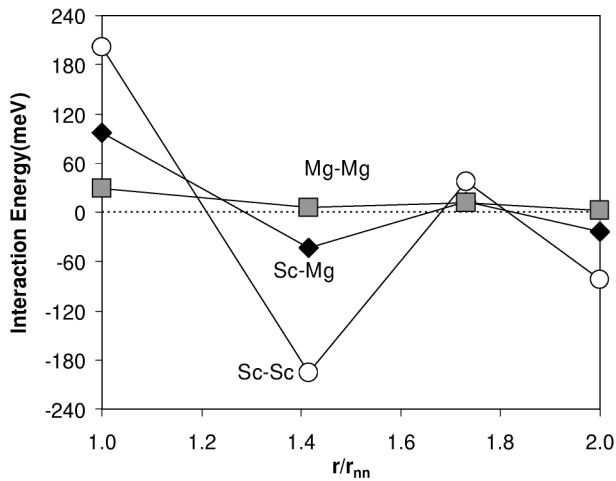


FIG. 4. Mg-Mg, Mg-Sc, and Sc-Sc interaction energies in an Al host, calculated as a function of separation  $r$  normalized by the nearest-neighbor distance  $r_{nn}$ .

The supercell calculations yield a preferred binding site for Mg that contains the maximum number of both second neighbors (one per Mg atom) and fourth neighbors (four per Mg atom) to interface Sc atoms, while featuring no nearest or third-nearest neighbor repulsive Mg-Sc pairs. From the calculated Mg-Sc interaction energies, assuming pair interactions are dominant, the binding energy of Mg to an  $\alpha$ -Al/Al<sub>3</sub>Sc {200} heterophase interface can be estimated to be 0.12 eV, in very close agreement with the direct supercell calculations. This result suggests that Mg segregation at the  $\alpha$ -Al/Al<sub>3</sub>Sc interface can be interpreted as reflecting the nature of Mg-Sc electronic interactions in Al. Interestingly, the results in Fig. 4 also suggest substantial crystalline anisotropy in the degree of equilibrium Mg segregation. Because of the higher areal densities of sites containing attractive second and fourth neighbor interactions with interface Sc atoms, Mg adsorption is estimated to be roughly a factor of 3 and 2.5 larger for {110} and {111} interfaces, respectively, relative to the lower-energy {100} orientation. From the Gibbs adsorption theorem, Mg segregation is thus predicted to lower the anisotropy of the  $\alpha$ -Al/Al<sub>3</sub>Sc interfacial free energy, consistent with the observed reduction in precipitate faceting induced by the addition of Mg (Fig. 1).

This research was supported by the Office of Science of the U.S. Department of Energy under Contracts No. DE-FG02-98ER45721 (E. M. and D. N. S.), No. DE-FG02-01ER45910 (M. A.), and resources at the National Energy Research Scientific Computing Center under Contract No. DE-AC03-76SF00098; the AFOSR under Contract No. F33615-01-C-5214 (C.W.); and the DOD High Performance Computer Modernization Program at the ASC-MSRC in the IBM-SP3. HREM was performed

at the Electron Microscopy Laboratory at Argonne National Laboratory. Professors D. C. Dunand and P. W. Voorhees are thanked for helpful discussions.

\*Present address: Sandia National Laboratories, Livermore, CA 94551, USA.

†Permanent address: Materials and Manufacturing Directorate, Air Force Research Laboratory, Wright Patterson AFB, OH 45433, USA.

- [1] L. S. Toporova *et al.*, *Advanced Aluminum Alloys Containing Scandium* (Gordon and Breach, Amsterdam, 1998).
- [2] E. A. Marquis and D. N. Seidman, *Acta Mater.* **49**, 1909 (2001).
- [3] E. A. Marquis, Ph.D. thesis, Northwestern University, 2002.
- [4] O. C. Hellman *et al.*, *Microsc. Microanal.* **6**, 437 (2000).
- [5] H. H. Jo and S. I. Fujikawa, *Mater. Sci. Eng. A* **171**, 151 (1993).
- [6] G. M. Novotny and A. J. Ardell, *Mater. Sci. Eng. A* **318**, 144 (2001).
- [7] C. J. Kuehmann and P. W. Voorhees, *Metall. Mater. Trans. A* **27**, 937 (1996).
- [8] V. Ozoliņš and M. Asta, *Phys. Rev. Lett.* **86**, 448 (2001).
- [9] M. Asta and V. Ozoliņš, *Phys. Rev. B* **64**, 094104 (2001).
- [10] C. Woodward *et al.*, *Phys. Rev. B* **63**, 094103 (2001).
- [11] S. I. Fujikawa, *Defect Diff. Forum* **143**, 115 (1997).
- [12] S. J. Rothman *et al.*, *Phys. Status Solidi B* **63**, K29 (1974).
- [13] M. Asta *et al.*, *Phys. Rev. B* **57**, 11 265 (1998).
- [14] Calculations were performed using the *ab initio* total-energy and molecular-dynamics program VASP (Vienna *ab initio* simulation package) developed at the Institut für Materialphysik of the Universität Wien [15,16]. Results in Fig. 3 were derived employing periodic supercell geometries in which the Al/Al<sub>3</sub>Sc interfaces were separated by 5–10 lattice constants, and Mg impurities were separated from nearest periodic images by four nearest-neighbor spacings. Solute interaction energies plotted in Fig. 4 were derived from periodic supercells in which solute atoms were separated from nearest periodic images by at least four nearest-neighbor spacings. The convergence of both sets of calculated results was estimated to be within a few times 0.01 eV.
- [15] G. Kresse and J. Hafner, *Phys. Rev. B* **47**, 558 (1993); **49**, 14 251 (1994).
- [16] G. Kresse and J. Furthmüller, *Comput. Mater. Sci.* **6**, 15 (1996); *Phys. Rev. B* **54**, 11 169 (1996).
- [17] F. Vurpillot *et al.*, *Appl. Phys. Lett.* **76**, 3127 (2000).
- [18] S. A. Dregia and P. Wynblatt, *Acta Metall. Mater.* **39**, 771 (1991).
- [19] B. W. Krakauer and D. N. Seidman, *Phys. Rev. B* **48**, 6724 (1993).
- [20] J. Zou and A. E. Carlsson, *Phys. Rev. B* **47**, 2961 (1993).
- [21] J. A. Moriarty and M. Widom, *Phys. Rev. B* **56**, 7905 (1997).